Chapter 5

Detection of trapped positrons

Positrons loaded into the trap through the off-axis entrance aperture dissipate energy in the LRC circuit until their axial motion comes into thermal equilibrium at 4 K. Their cyclotron energy similarly cools to 4 K via synchrotron radiation. Their magnetron motion, however, remains unchanged ($\rho_{\mathrm{mag}} \simeq \rho_h = 0.14$ inch) unless they are driven by a resonant radio frequency field. After positrons have been accumulated for a suitable length of time (typically several minutes or a few hours), they can be detected and counted through their coupling to the LRC circuit, as described in Section 5.1. In order to accurately count the number of positrons in the trap, it is necessary to move them from their large initial magnetron orbit to the center of the trap ($\rho = 0$). The technique for accomplishing this is described in Section 5.3. It is also important to measure the coupling strength between the LRC circuit and a *single* positron (or electron) in order to calibrate the positron counting technique (Section 5.4). The error bars quoted for number of trapped positrons and the positron loading rates are explained in Section 5.5.

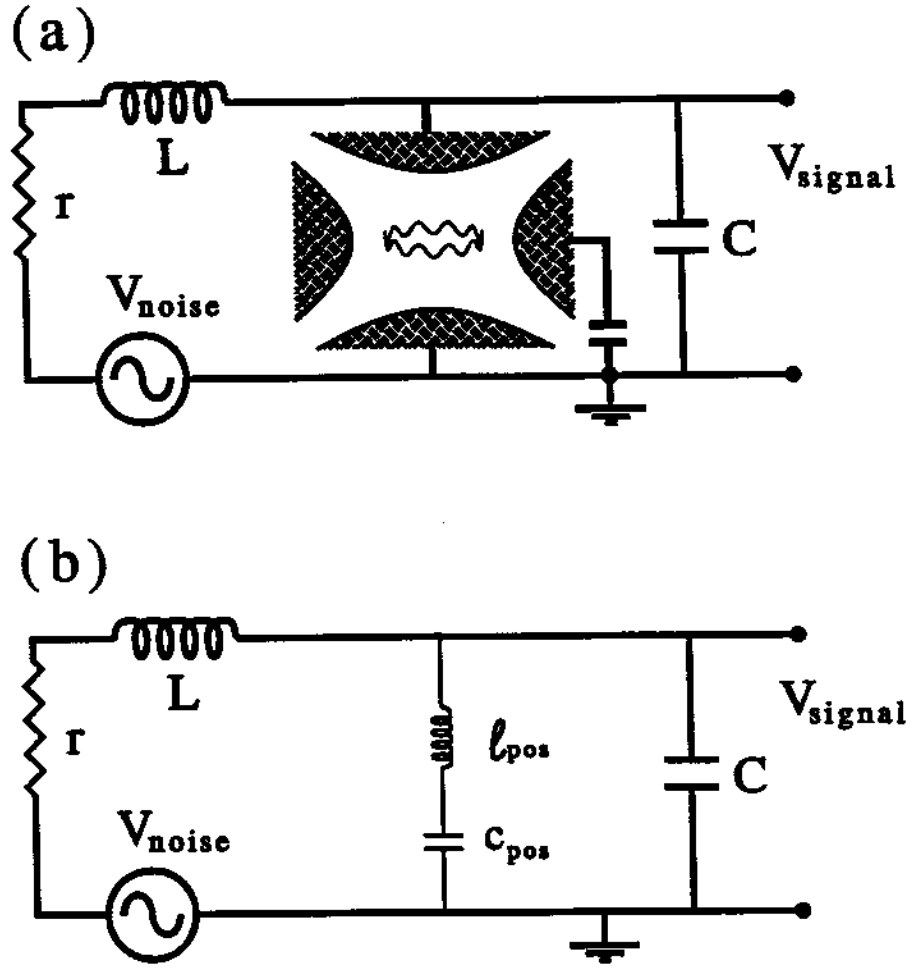

Figure 5.1: (a) Trapped positrons and the detection circuit are coupled harmonic oscillators. This is mathematically equivalent to a circuit (b) where the positrons are replaced by an inductor and a capacitor of the appropriate values [45].

5.1 Counting the positrons

The details of the interaction between trapped particles and a detection circuit have been explained elsewhere [45,50], and we give only a brief review here. The

axial motion of the positrons produces small oscillating image charges on the endcap electrodes, which in turn cause small currents to flow through the inductor L. The inductor has a small series resistance r which represents radiofrequency losses in the inductor and the rest of the detection circuit. Johnson noise in the circuit induces voltages on the endcap electrodes, to which the positrons respond. This is mathematically equivalent to the circuit shown in Fig. 5.1 when we choose [45]

$$\ell_{\rm pos} = Nm\left(\frac{2z_0}{\alpha e}\right)^2 \tag{5.1}$$

and

$$c_{\rm pos} = \frac{1}{\omega_z^2 \ell_{\rm pos}}, \tag{5.2}$$

where N is the number of positrons, $2z_0$ is the distance between the endcap electrodes, and α is a dimensionless quantity ≈ 0.5 for this trap geometry.

We now use the standard techniques of circuit analysis to determine the expected detection signal V_S. When the trap is empty, we obtain

$$|V_S(\omega)|^2 = \frac{|V_{\rm noise}|^2 \omega_{LC}^4}{(\omega_{LC}^2 - \omega^2)^2 + \omega^2\Gamma^2}, \tag{5.3}$$

where $|V_{\rm noise}|^2 = 4k_BT\,r\,\Delta\nu$ is the familiar Johnson noise at temperature T. For $\omega \approx \omega_{LC}$ this gives the Lorentzian form

$$|V_S(\omega)|^2 = \frac{|V_{\rm noise}|^2 Q^2 (\Gamma/2)^2}{(\omega_{LC} - \omega)^2 + (\Gamma/2)^2}, \tag{5.4}$$

where Q is the quality factor of the circuit and $\Gamma = r/L$ is the usual full-width half-maximum of $|V_S|^2$. An example of the noise spectrum for an empty trap is shown in Fig. 4.16. When there are positrons in the trap, Eq. 5.3 becomes [51]

$$|V_S(\omega)|^2 = \frac{|V_{\rm noise}|^2 \omega_{LC}^4 (\omega_z^2 - \omega^2)^2}{\left[(\omega_z^2 - \omega^2)(\omega_{LC}^2 - \omega^2) - \omega^2\Gamma N\gamma_z\right]^2 + \omega^2\Gamma^2\left[(\omega_z^2 - \omega^2) + \Gamma N\gamma_z\right]^2}, \tag{5.5}$$

where, as before, N is the number of trapped positrons, ω_z is their axial frequency (which need not necessarily equal ω_{LC}), and γ_z is the damping constant for the positron axial motion which we calculated in Section 4.3.

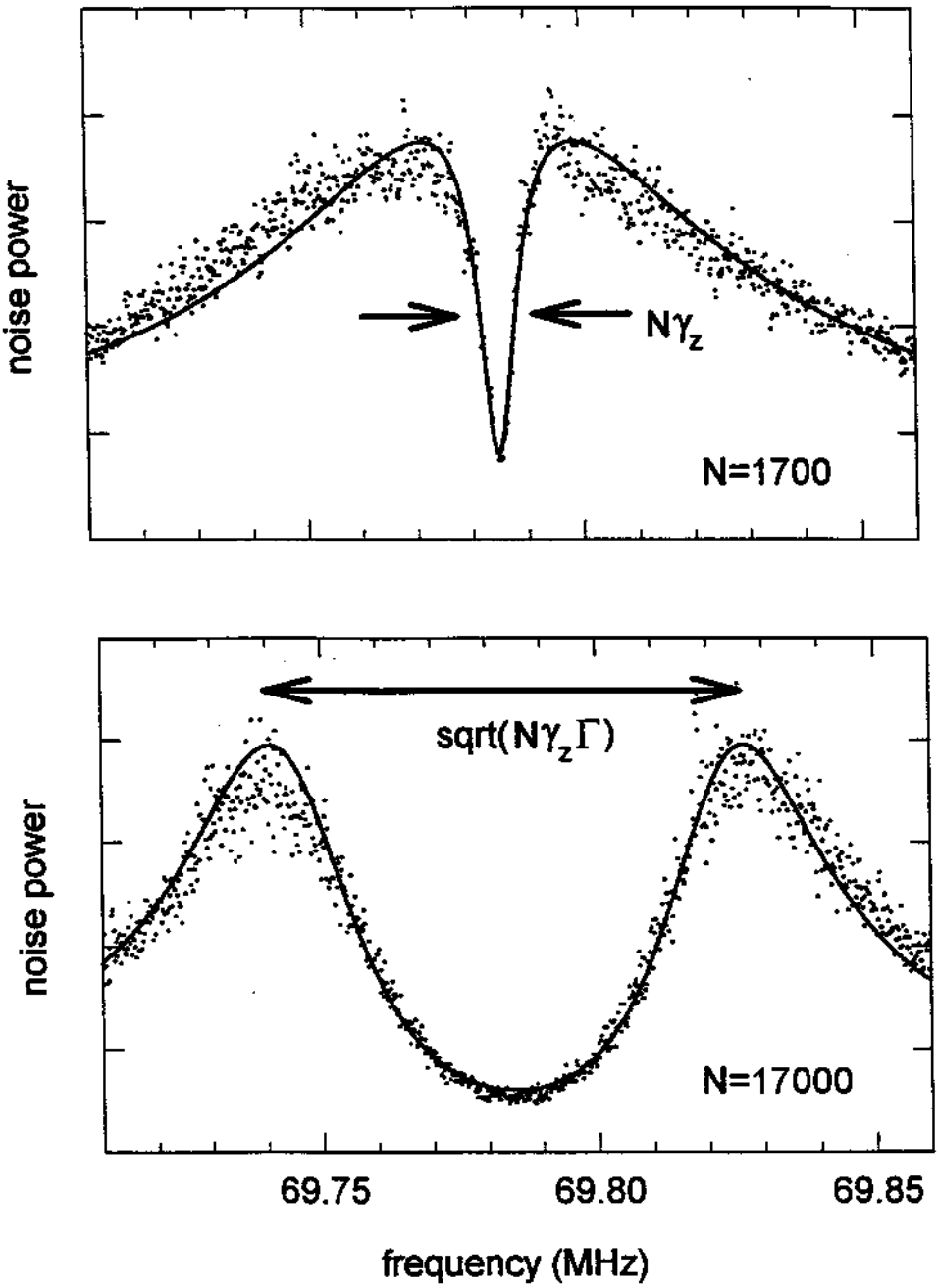

Figure 5.2: Typical noise spectra obtained from trapped positrons and the LRC detection circuit. The darker lines are least-squares fits of the theoretical lineshape. (a) Spectrum with 1700 trapped positrons. The FWHM of the "dip" is approximately equal to $N\bar{\gamma}_z$. (b) Spectrum with 17,000 trapped positrons. The maxima in the signal are separated by approximately $\sqrt{N\bar{\gamma}_z\Gamma}$.

To obtain some intuitive understanding of Eq. 5.5, we examine two limiting cases. When the number of positrons is small ($N\gamma_z \ll \Gamma$) and $\omega_z = \omega_{LC}$, Eq. 5.5 reduces to [50]

$$|V_S(\omega)|^2 \propto |V_{\text{noise}}|^2 \left[1 - \frac{(N\gamma_z/2)^2}{(\omega_z - \omega)^2 + (N\gamma_z/2)^2}\right] \tag{5.6}$$

near resonance ($\omega \approx \omega_z$). This is essentially an inverted Lorentzian "dip" in the peak noise signal with a FWHM equal to $N\gamma_z$. An example of this is shown in Fig. 5.2. The width of the "dip" is proportional to the number of trapped positrons. The other limiting case is for large N (with $\omega_z = \omega_{LC}$), also shown in Fig. 5.2; the maxima in the noise spectrum occur at frequencies

$$\omega^{\pm} \simeq \omega_{LC} \pm \frac{1}{2}\sqrt{N\gamma_z\Gamma}. \tag{5.7}$$

The separation between the maxima grows as $\sqrt{N}$.

To count the number of positrons in the trap, the noise spectra of the trapped particles and circuit are fit to the theoretical lineshape of Eq. 5.5. The least-squares curve fitting takes ω_{LC}, Γ, and γ_z as fixed parameters and adjusts ω_z (the minimum point of the dip) and N (the number of positrons) to obtain a best fit. Examples of best-fit curves are included in Fig. 5.2. The uncertainties in this measurement are discussed in Section 5.5.

5.2 Amplifying the detection circuit signal

The electrical signal produced by the positrons' axial motion and by the Johnson noise in the LRC circuit is very weak and requires a great deal of amplification before it can be analyzed. The inductor is contained in a helical resonator cavity to increase the quality factor of the circuit. We use a dual-gate, gallium arsenide FET as our first stage of amplification. The gate-1 input of the FET is capacitively connected to the inductor at approximately its midpoint. The FET, like the inductor and trap electrodes, is cooled by thermal contact to a liquid helium

reservoir to reduce thermal noise. The drain lead of the FET is impedance matched through a pi network matching circuit to a 50 Ω micro-coax cable, which carries the signal to a vacuum feedthrough on the magnet's "hat" (pictured in Fig. 2.4). The signal then goes through about 100 dB of commercially available low-noise broadband amplifiers. A more detailed description of the GaAs FET, including a wiring diagram, is contained in Refs. [23], [24], and [50].

After the signal is amplified, we analyze and store it on computer by one of two methods: (1) through the use of a commercial spectrum analyzer; (2) by mixing the signal to 5 MHz using a (frequency-swept) local oscillator, then sending the signal through a crystal filter (with a bandwidth of $\sim$ 7 kHz) and a square law detector. (The second method is only useful when the width of the "dip" produced by the trapped positrons is greater than the bandwidth of the crystal filter.) Both methods produce noise spectra such as are shown in Fig. 5.2.

5.3 Moving the positrons to the trap's central axis

It is difficult to detect trapped positrons when they are allowed to remain in their initial distribution of large magnetron orbits ($\rho_h - r_e \leq \rho_{\mathrm{mag}} \leq \rho_h + r_e$). Although it is possible to detect large off-axis clouds (more than 1000 particles) by the "dip" they produce in the noise spectrum, the dip is usually quite shallow and spread over a large frequency range. This, presumably, is due to inhomogeneities in the quadrupole potential. It is preferable to move the positrons to the center of the trap ($\rho \approx z \approx 0$), where the inhomogeneities are less important and all of the positrons move with nearly the same axial frequency. The positrons' axial motion cools to equilibrium at 4 K so long as $\omega_z \approx \omega_{LC}$. The process of shrinking the positrons' magnetron motion radius is typically called "magnetron sideband cooling."

Magnetron cooling is described elsewhere (see Refs. [52,53]), including detailed calculations of the cooling rate [22]. We give a brief description here. Since the magnetron motion is energetically unstable, it is necessary to *add* energy to this motion to reduce the magnetron quantum number and to decrease its radius. This is accomplished by applying, to one quadrant of the bottom compensation electrode, a sideband excitation drive at the frequency $\nu_z + \nu_m$. As the positrons absorb energy from this drive, both their magnetron and axial motions gain energy. The axial motion is damped by coupling to the LRC circuit, so the net effect of applying this drive is a gradual increase of the magnetron energy and a gradual shrinking of the magnetron motion radius. The cooling continues until we reach the condition [22,54,55]

$$\langle E_{\mathrm{mag}} \rangle = -\frac{\omega_m}{\omega_z} \langle E_{\mathrm{axial}} \rangle. \tag{5.8}$$

For axial motion cooled to 4 K, magnetron cooling stops when $\rho_{\mathrm{mag}} \approx 10^{-4}$cm. Figure 5.3 shows an example of the noise spectrum of a small positron cloud with the magnetron cooling drive applied. It is important that the magnetron cooling drive not be too strong, or otherwise it heats the axial motion faster than the LRC circuit can damp the energy, and the positrons are driven out of the trap. Conversely, if the cooling drive is too weak, it takes a very long time to move the positrons to the center of the trap.

Because of the inhomogeneities in the trap's quadrupole potential, we cannot expect the positron's axial frequency ν_z to be the same for all values of ρ_{mag}. In fact, depending upon V_{comp}, ν_z can vary by several hundred kilohertz between $\rho_{\mathrm{mag}} = 0$ and $\rho_{\mathrm{mag}} = \rho_h$. Therefore, we cannot expect to use a single drive frequency to cool the positrons all the way to the center of the trap.

Since this Penning trap was designed to be "orthogonalized" [26,43], we expect only a very small shift in ν_z for on-axis positrons as V_{comp} is adjusted. In fact, we measure

$$\frac{\Delta \nu_z}{\nu_z} = +3 \times 10^{-4} \frac{V_{\mathrm{comp}}}{V_{\mathrm{ring}}} \tag{5.9}$$

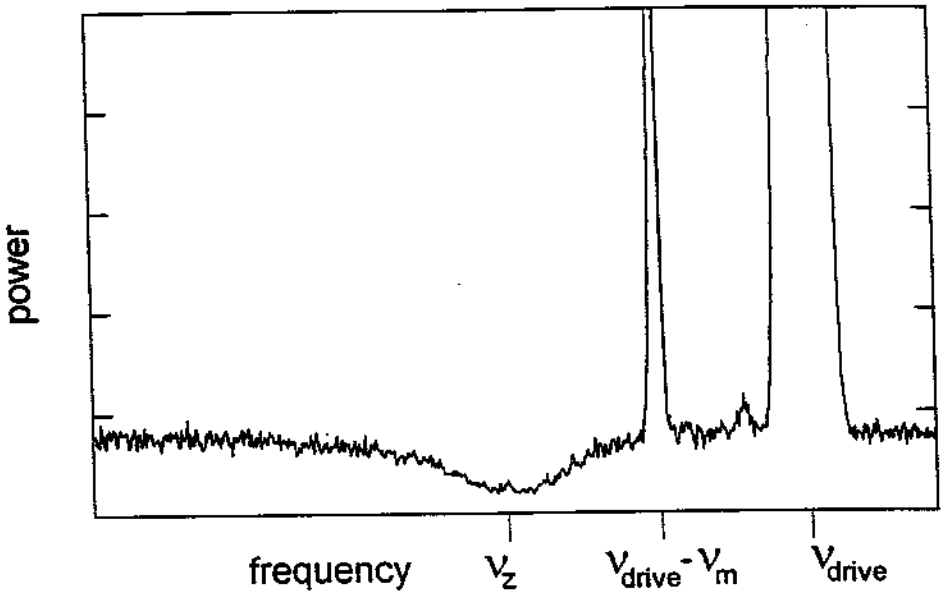

Figure 5.3: Noise spectrum of trapped positrons with the magnetron sideband cooling drive applied. The dip in the noise power is caused by the response of the trapped positrons to Johnson noise in the circuit; its center is at the axial frequency of the trapped positrons. The large signal to the right of the dip is the cooling drive. The "spike" at the right edge of the dip shows the axial motion of the positrons being excited at $\nu_{\text{drive}} - \nu_m$ in response to the drive.

for small numbers of positrons (< 500) trapped on-axis. We see from Fig. 4.15 that for off-axis positrons ($\rho = \rho_h$) in small axial orbits ($z_{\text{max}} < z_0$), we theoretically expect

$$\frac{\Delta\nu_z}{\nu_z} = -1 \times 10^{-2} \frac{V_{\text{comp}}}{V_{\text{ring}}}, \tag{5.10}$$

which is much larger in magnitude and of the opposite sign as the on-axis value.

Although it is possible to adjust V_{comp} so that ν_z is the same for both the on-axis and off-axis locations, we could not be certain that ν_z would remain constant for every radius in between. We choose instead to set $V_{\text{comp}} = 0$ Volts, which

we know empirically causes ν_z (*off axis*) $\simeq$ ν_z (*on axis*) + 400 kHz, and presumably ν_z should change monotonically for all intermediate values of ρ. We then fix V_{ring} and "sweep" the sideband cooling drive frequency slowly downward from ν_z (*off axis*) + ν_m to ν_z (*on axis*) + ν_m, which keeps the cooling drive resonant with the positrons continuously as they move to the center of the trap. Alternatively, we adjust V_{ring} so that initially $\nu_{LC} = \nu_z$ (*off axis*), and keep the cooling drive fixed at $\nu_{LC} + \nu_m$ while slowly sweeping V_{ring} upward until $\nu_{LC} = \nu_z$ (*on axis*), at which point the positrons are centered in the trap. We prefer the latter method because it maximizes the LRC circuit's damping of the axial motion throughout the magnetron cooling process.

In order to maximize the efficiency of the magnetron cooling sweep, and to ensure that we center *all* of the loaded positrons, we tested our procedure on (nearly) identical positron clouds (each loaded for equal lengths of time using identical settings) for a variety of different "sweep" settings. Those results are shown in Fig. 5.4. For each data point, the cooling drive frequency was fixed at $\nu_{LC} + \nu_m$ and V_{ring} was swept from some initial setting to a fixed final value which caused $\nu_{LC} = \nu_z$ (*on axis*). We varied the V_{ring} sweep range, the V_{ring} sweep rate, and the cooling drive power. The first graph shows the number of positrons moved to the center of the trap as a function of the V_{ring} sweep range, with a fixed (slow) sweep rate (0.1 mV per second), for a variety of different cooling drive strengths. The second graph shows the number of positrons moved to the center of the trap as a function of the total V_{ring} sweep time, for fixed V_{ring} sweep range (0.18 Volts), for a variety of different cooling drive strengths. The results show that if the sweep range is too small, or if the sweep rate is too fast, some of the positrons are not centered.

We understand these results as follows: The value of V_{ring} at the beginning of the cooling sweep must be sufficiently far from the final value so that

$$\nu_z \text{ (off axis)} < \nu_{LC} + \nu_m \tag{5.11}$$

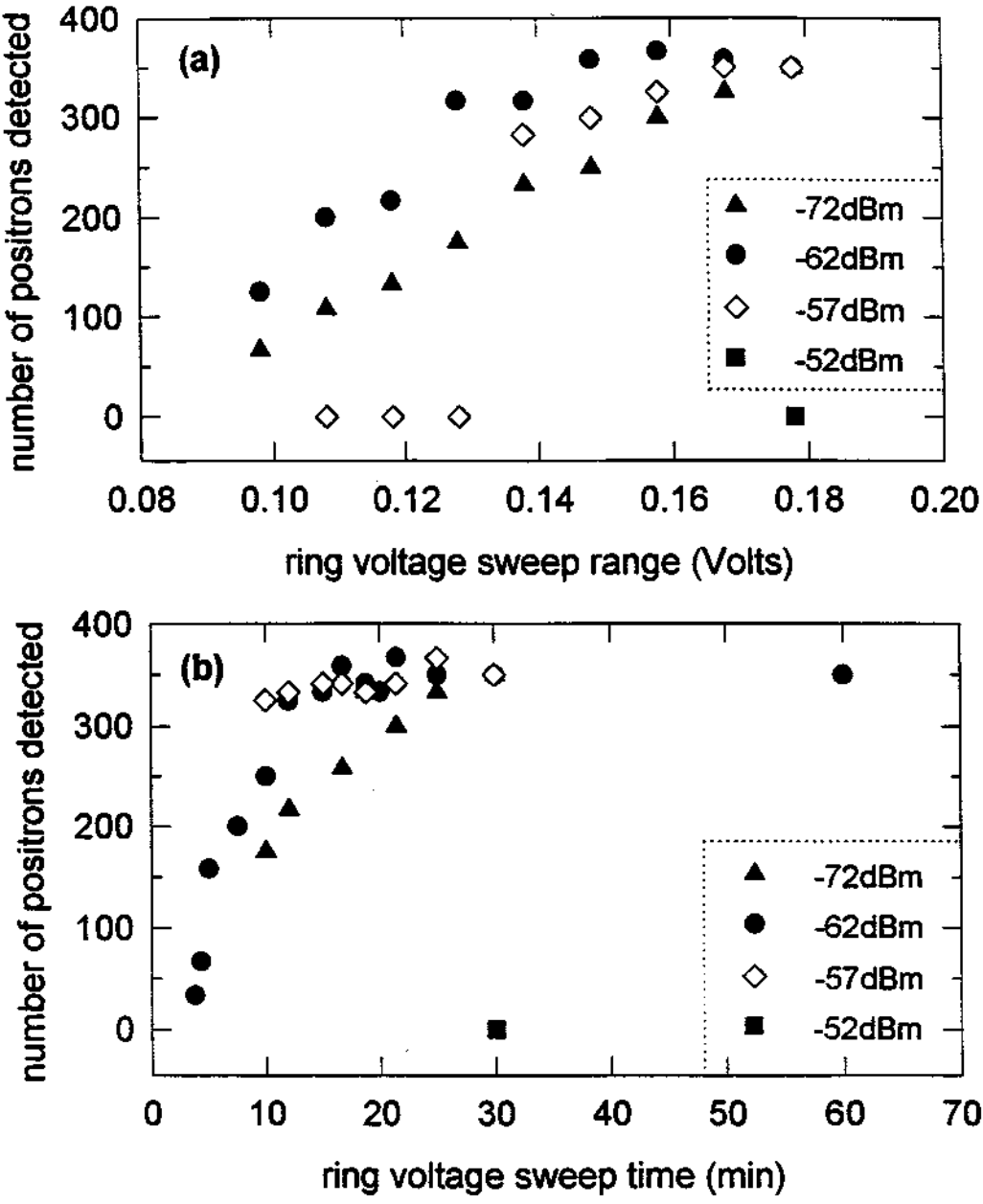

Figure 5.4: Magnetron cooling procedures for various cooling drive strengths. (a) The number of positrons moved to the center of the trap *vs.* the range of the V_{ring} sweep, at a fixed sweep rate (0.1 mV per second) and a fixed final ring voltage. (b) The number of centered positrons *vs.* the total sweep time, for a fixed ring voltage sweep range (0.18 V).

for *all* positrons loaded into the trap. If the initial value of V_{ring} is too close to the final value (*i.e.* the sweep range is too small), some of the positrons have ν_z (*off axis*) $\geq \nu_{LC} + \nu_m$; those positrons are magnetron *heated* by the drive and move *away* from the center of the trap. This explains why fewer positrons are centered when the V_{ring} range is small. Even when Eq. 5.11 holds for all positrons in the trap, not all of the positrons have sufficient time to cool to the trap center if the V_{ring} sweep *rate* is too fast, as shown in graph (b). Note that stronger drive strengths cool the positrons more quickly, allowing for a faster sweep rate. (A drive strength of −72 dBm requires at least 25 minutes to center all of the positrons, compared to 15 minutes at −62 dBm.) If, however, the drive is too strong (> -52 dBm), all of the positrons are lost.

We therefore choose a V_{ring} sweep range of 0.18 Volts, a total sweep time of 15 minutes, and cooling drive power of −62 dBm for all measurements of the positron loading rate. During the magnetron cooling sweep and also at all other times, both V_{ring} and V_{comp} are controlled through low-pass RC filters with a ten-second time constant. The cooling drive strengths listed are the strengths applied to the vacuum feedthrough at the magnet's "hat." Some small losses in power are expected in the 200 Ω twisted pair wires used to carry the signal to the vacuum feedthroughs on the trap can.

It is possible to detect the presence of even a small number of trapped positrons (< 20) during the magnetron cooling sweep, before they have been fully centered. Recall from Fig. 5.3 that, as the magnetron cooling drive heats the positron's axial motion, a "response spike" appears in the noise spectrum at one magnetron frequency sideband below the cooling drive. Often, more sidebands appear at several multiples of ν_m below the cooling drive. We monitor this signal on a spectrum analyzer during the early stages of the magnetron cooling sweep. The presence or absence of a "response spike" at the magnetron sideband is often the first indication of trapped positrons, even before a "dip" appears.

When ions are present in the trap along with positrons, the response spike

during the magnetron cooling sweep is small or non-existent until the very end of the cooling sweep. At the end of a cooling sweep with ions, no dip forms in the noise spectrum, but rather a broad ($\sim$ 1 kHz) "hump" appears in response to the sideband excitation drive.

5.4 Measuring a single positron (electron)

The use of Eq. 5.5 to count the number of trapped positrons requires knowledge of γ_z, the damping constant for a single positron. In principle, one could load a single positron (or electron) into the center of the Penning trap and measure the FWHM of the "dip" in the noise spectrum. This has recently been done in an essentially identical Penning trap with an electron [56]. The signal-to-noise caused by a single positron or electron is small, so that several minutes of integration and signal averaging are required to resolve this dip. Unfortunately, the stability of the voltage source used for V_{ring} in this experiment is inadequate. During the course of several minutes it typically drifts several tenths of a microVolt, which causes ω_z to drift several times the value of γ_z. While this small voltage drift does not affect the positron loading rate or the ability to accurately measure large clouds of positrons, it does make it impossible to directly measure γ_z by this method.

The signal-to-noise of a single trapped particle can be increased by applying a resonant axial drive and measuring the response using phase-sensitive detection [22]. We adjust V_{ring} so that $\omega_z = \omega_{LC}$ and drive the trapped particle at ω, thereby observing a signal

$$V_S(\omega) \propto V_D \frac{(N\gamma_z/2)^2 \cos\phi + (N\gamma_z/2)(\omega_z - \omega)\sin\phi}{(\omega_z - \omega)^2 + (N\gamma_z/2)^2}, \tag{5.12}$$

where V_D is the drive amplitude, N is the number of trapped particles, and ϕ is the (adjustable) relative phase between the drive and the forced response. At $\phi = 0°$ and $\phi = 90°$, we obtain the familiar absorption and dispersion response curves for damped, driven harmonic oscillators. Note that the FWHM of the

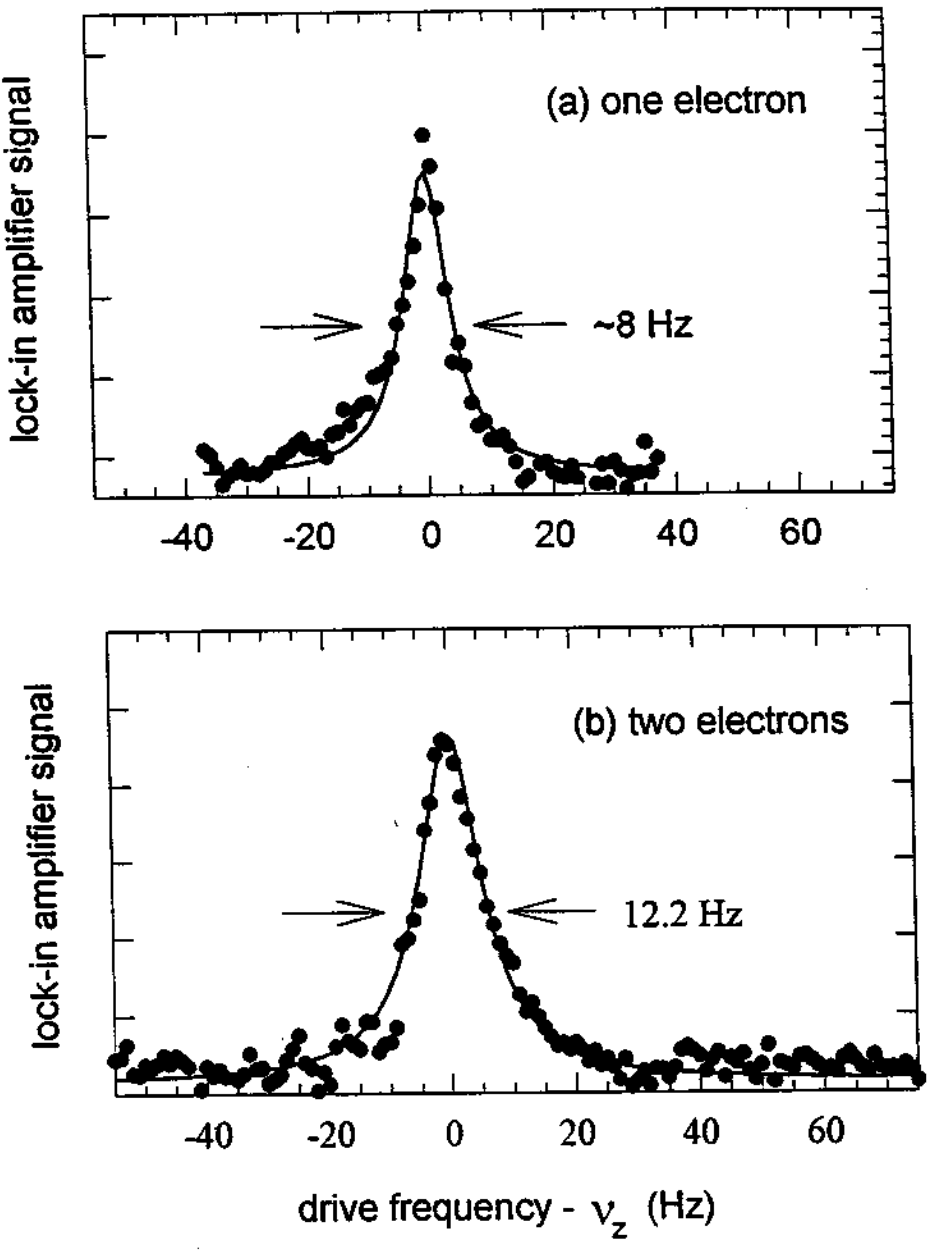

Figure 5.5: Driven response detection of (a) one trapped electron; (b) two trapped electrons. The solid curves are best-fit Lorentzians. Due to drifts in the trapping voltage, the single-electron absorption curves do not fit a Lorentzian lineshape as well as those of larger clouds.

absorption curve is $N\gamma_z$.

Under typical operating conditions, we apply a 5 MHz drive at –27 dBm power to the ring electrode and frequency sweep a second drive around $\nu_z - 5$ MHz at –17 dBm power applied to the bottom endcap. The driven response signal of the particle at $\sim \nu_z$ is mixed with the bottom endcap drive signal, filtered through a 5 MHz bandpass crystal filter, and connected to the input of a commercial lock-in amplifier. The 5 MHz drive applied to the ring electrode also provides the reference signal for the lock-in amplifier. Figure 5.5 shows examples of the output of the lock-in amplifier as a function of the driving frequency for (a) one and (b) two electrons in the trap and $\phi = 0°$. Because this method produces a larger signal-to-noise than an undriven electron, it takes much less integration and averaging time to obtain a good measurement than using the noise-spectrum technique of Section 5.1. Thus, we can make a measurement of γ_z before V_{ring} drifts significantly.

We determined γ_z by using the on-axis FEP to load a variety of small clouds into the center of the trap, ranging from one to nine electrons. (This technique is much quicker than loading and centering small clouds of positrons.) For each cloud, three or four different absorption curves were taken of the type pictured in Fig. 5.5. For each sweep, the FWHM of the lock-in signal was measured, and the results were averaged (to reduce the effect of V_{ring} drift on any particular sweep). The horizontal axis of Fig. 5.6 shows the measured widths for these clouds, which cluster at multiples of 6.1 Hz with the exception of four clouds (all of them < 17 Hz in width) which are broadened due to trapping voltage instability. The broadened clouds did not produce lineshapes which fit the Lorentzian form as well as the clouds whose FWHM clustered around multiples of 6.1 Hz. The instability in V_{ring} proved too great to obtain a good measurement of $N\gamma_z$ on single-electron clouds (and on one occasion for two electrons). Fortunately, we have a fair number of absorption curves, with nice Lorentzian shapes, with FWHM of $\sim$ 12.2 Hz, 18.3 Hz, and 24.4 Hz.

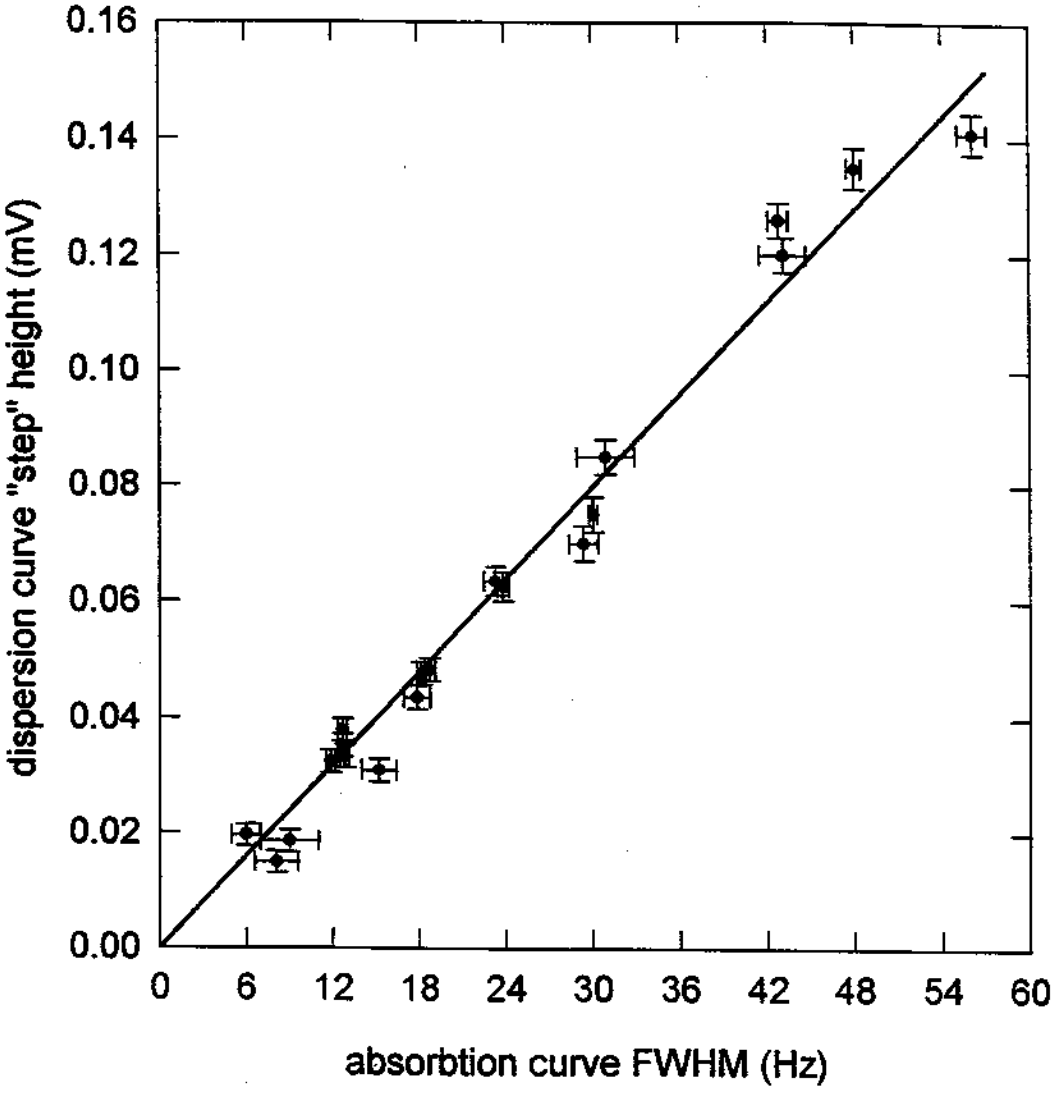

Figure 5.6: Comparison of the FWHM of the absorption curve (horizontal axis) with the height of the "step" in the dispersion curve (vertical axis) for 20 different clouds ranging from 1 to 9 electrons. The absorption FWHM ($= N\gamma_z/2\pi$) are clustered at multiples of 6.1 Hz.

In Penning traps which have a sufficiently stable voltage supply for V_{ring}, it is possible to use the lock-in signal to literally "watch" electrons load into the trap one at a time. (See for example Ref. [57].) Note from Eq. 5.12 that for large detuning in the drive frequency $|\omega - \omega_z| \gg N\gamma_z$, the dispersive component of the lock-in signal ($\phi = 90°$) is proportional to the number of electrons in the trap. By monitoring this signal continuously while the on-axis FEP is fired at a low current, it is possible to see the lock-in signal discontinuously jump each time an additional electron is trapped [50].

Because of the greater instability of V_{ring} in our trap already mentioned, we used a variation of this technique. After the measurements of the absorption curve were taken for each cloud, we rapidly shifted the endcap drive frequency to 400 Hz below resonance and increased the drive strengths by 15 dB, after which the dispersion curve ($\phi = 90°$) lock-in signal was monitored for 90 seconds. At the end of those 90 seconds, V_{ring} was adjusted to shift the electron(s) much farther out of resonance (several kHz), which gave the baseline signal level, which was also monitored for 90 seconds. The results of this procedure for most of the clouds used in Fig. 5.6 is shown in Fig. 5.7. The size of this "step" in the dispersion response for each cloud is shown on the vertical axis of Fig. 5.6, and in each case it clusters around values which are correlated with the measured FWHM of the absorption curve.

By using Fig. 5.6 to determine the number of electrons in each cloud, and averaging the measured values of the $N\gamma_z$ for each N, we obtain Fig. 5.8. The value of the best-fit line at $N = 1$ gives us a measured value of $\gamma_z/2\pi = 6.1 \pm 0.1$ Hz. All of these measurements were taken with an LRC circuit quality factor of $Q = 990$.

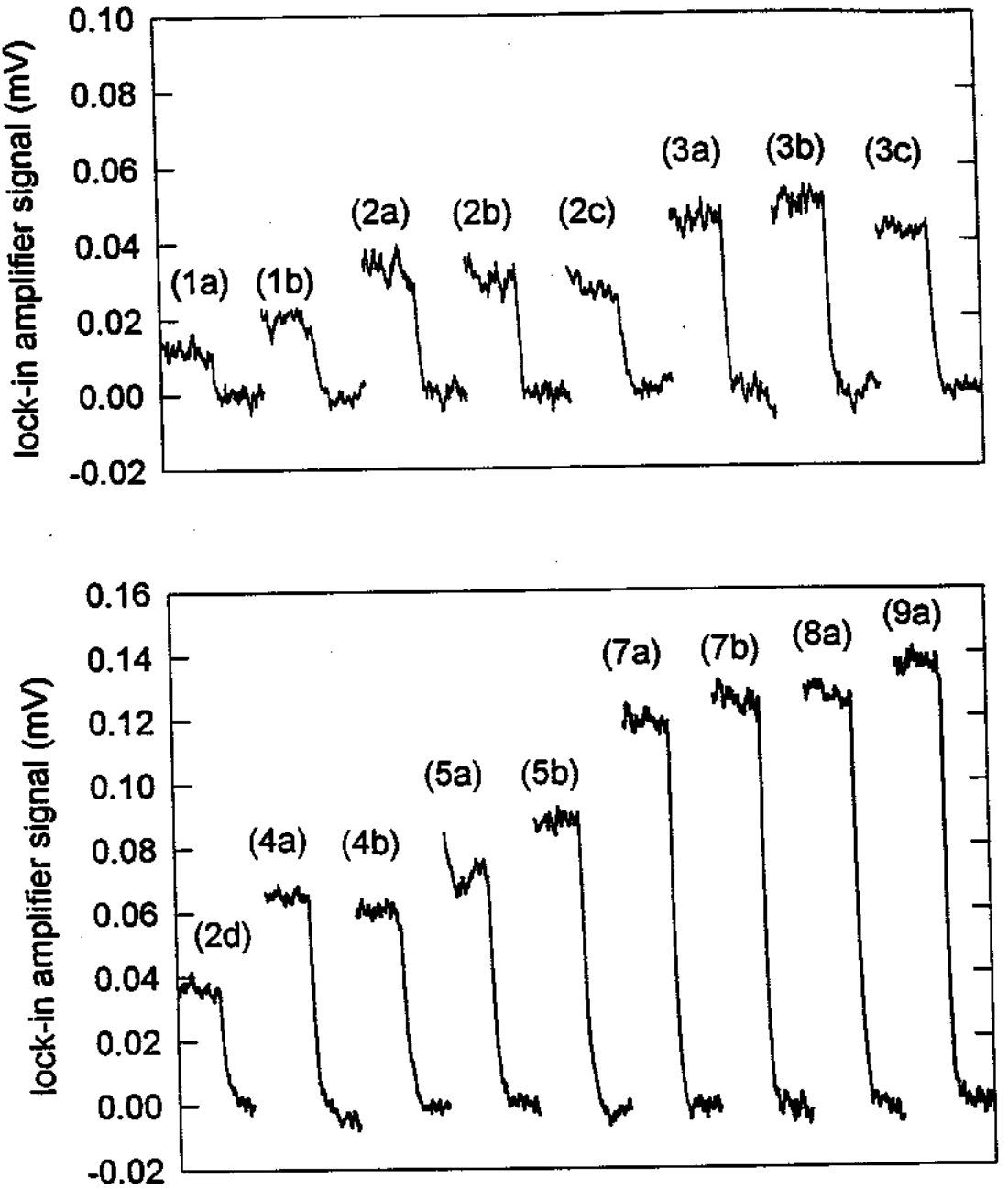

Figure 5.7: The far off-resonance dispersion ($\phi = 90°$) response of the small electron clouds used to measure γ_z.

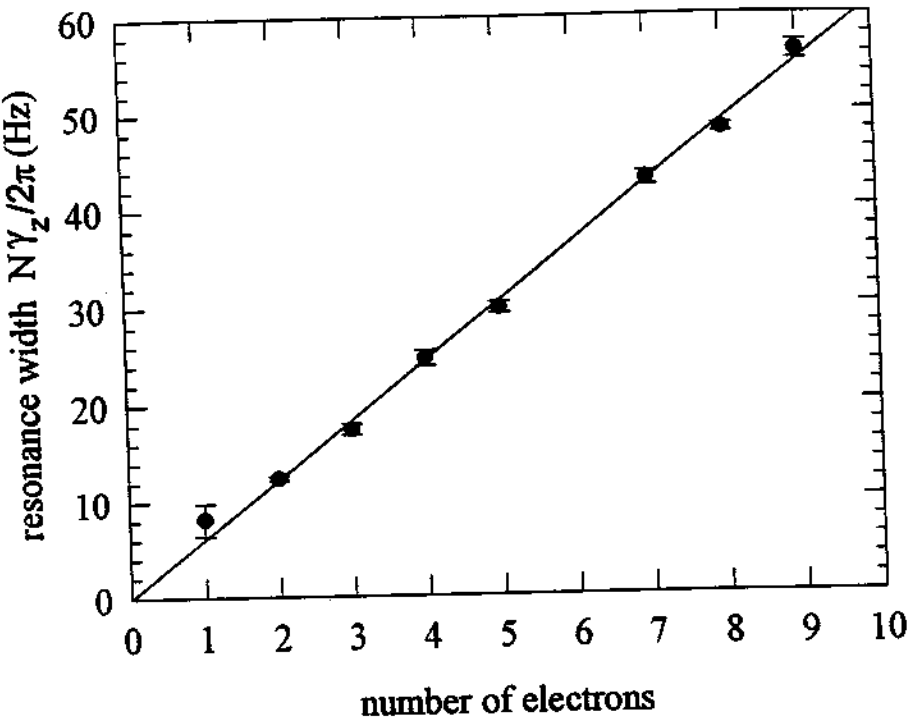

Figure 5.8: The averaged values of $(N\gamma_z/2\pi)$ for each N, where N is the number of trapped electrons and $(N\gamma_z/2\pi)$ is the FWHM of the absorption curve.

5.5 Measuring the loading rate and estimating errors.

All measurements of the positron loading rate presented in the previous chapters were taken with a total positron accumulation time of 35 minutes per data point. At the beginning of each loading cycle, V_{ring}, V_{comp}, V_{tube}, and V_{mod} were set to their chosen values and the mechanical beam shutter was opened. While positrons accumulated, a drive applied to the bottom endcap electrode resonantly drove out positive ions which might also accumulate (Section 4.7). At the end of 35 minutes, the mechanical beam shutter was closed and the ion drive was turned off. The

magnetron sideband cooling drive was then applied to move the positrons to the center of the trap, as described in Section 5.3. Finally, the noise spectrum of the LRC circuit and positrons was taken with a spectrum analyzer or a square law detector, and the spectrum was stored. The positrons were then dumped out of the trap by biasing V_{ring} and V_{comp} positively and the process was repeated. The entire procedure took approximately one hour per cycle. The loading rate was calculated by dividing the number of trapped positrons—as determined by least-squares fit to the noise spectrum—by the accumulation time.

For clouds of 1000 positrons or more, independent noise spectra of the same cloud yield slightly different values of N when fit to the theoretical lineshape, with a standard deviation of about 1%. For smaller clouds, the standard deviation proved to be ~ 10 positrons. (Clouds of fewer than 10 positrons did not produce dips which could be fit to the theoretical lineshape.) Our error estimate for lineshape fitting is therefore 1% of N for $N > 1000$ and 10 otherwise. There is also an uncertainty of 1.6% in γ_z, which we add in quadrature. When the positron loading *rate* is measured, an additional factor of $\sqrt{N}$ is added in quadrature to the error estimate due to shot noise.

The pi network impedance matching circuit on the output of the GaAs FET (Section 5.2) slightly changes the shape of the LRC circuit's noise spectrum. The Lorentzian shape of the LRC's noise (with $Q \simeq 750$) is superimposed on a much broader ($Q \simeq 10$) Lorentzian lineshape of the pi network. This is accounted for in the lineshape fitting by a small quadratic background term, although the effects of including this term on the calculated value of N are not significant.